Wide-Range Calibration of Magnetic Moments for Vibrating Sample Magnetometers

Zhigao Zhang, Zhiyi Xu, Jian He, and Jun Lu

***Abstract*— Vibrating sample magnetometers (VSMs) have been widely used in the characterization of industrial magnetic materials, and their reliability is dependent on proper calibration. To improve the precision and range of calibration for VSMs, current-carrying microcoils were used to produce a tunable magnetic moment over a wide range. Based on comprehensive designing, we built a detection coil set of 0.3% uniformity in 8 mm along vibration direction. The calibration chain via moment coils of 2.5 mm diameter and height has been linked up between Ni spheres and the quantum benchmark. The differential magnetic moment due to a change in the applied current was used for calibration without dependence on the magnetic field. Magnetic moments with ranges across four orders of magnitude were calibrated and compared to those of the nickel standard and slope method. *In situ* calibration of a wide range of magnetic moments for VSMs without dependence on the field and materials was established, and the typical relative standard error did not exceed 0.3% within the range of 2.5–3.7 memu.**

***Index Terms*— Magnetic moment calibration, quantum traceability, vibrating sample magnetometer (VSM).**

I. Introduction

VIBRATING sample magnetometers (VSMs) have been developed and widely used for investigating the magnetostatic properties of matter since the 1950s [1], [2]. In comparison to force-based instruments such as magnetic balances and flux measurement equipment such as the superconducting quantum interference device (SQUID), VSMs possess great advantages in terms of the measurement range of the magnetic moment, sensitivity, operational convenience, and compatibility of the environment for magnetic materials [3], [4]. As a result, VSMs have become a standard instrument for characterizing industrial magnetic materials, and they can be properly applied in various electronic devices, such as inductors, transformers, and motors [5].

Manuscript received 29 April 2022; revised 9 June 2022; accepted 28 July 2022. Date of publication 5 August 2022; date of current version 18 August 2022. This work was supported in part by the National Key Research and Development Program of China under Grant 2021YFF0701000 and Grant 2018YFF0212603, in part by the National Natural Science Foundation of China under Grant 51327806 and Grant 12174425, in part by Fujian Institute of Innovation and Youth Innovation Promotion Association of Chinese Academy of Sciences under Grant 2018009, and in part by the Key Research Program of the Chinese Academy of Sciences under Grant ZDRW-CN-2021-3. The Associate Editor coordinating the review process was Dr. Branislav Djokic. *(Zhigao Zhang and Zhiyi Xu contributed equally to this work.) (Corresponding author: Jun Lu.)*

Zhigao Zhang and Jian He are with the National Institute of Metrology, Beijing 100029, China.

Zhiyi Xu and Jun Lu are with the State Key Laboratory of Magnetism, Institute of Physics, Chinese Academy of Sciences, Beijing 100190, China (e-mail: lujun@iphy.ac.cn).

Digital Object Identifier 10.1109/TIM.2022.3196952

The accuracy and reliability of VSM measurements are crucial for large-scale industrial applications. In comparison to magnetic steels with special shapes and sizes above 1 cm, the testing standards for which have been covered by the IEC 60404 series, magnetic samples with millimeter or submillimeter dimensions lack a calibration standard for moment measurement with an uncertainty below 1% [6], [7]. As early as the 1960s, National Institute of Standards and Technology (NIST) introduced two VSM calibration methods: the comparison method and slope method [8]. The comparison method uses the saturated magnetic moment of a standard nickel ball as the reference object to calibrate the magnetic moment, and the slope method uses materials with high magnetic permeability ($\mu_r \geq 2000$), where the magnetic moment and the external magnetic field are correlated and calibrated simultaneously by using the linear dependence of the observed magnetic moment on the applied field over the lower region of the magnetization curve [8].

The magnetostatic force method has also been taken as an independent method of calibration for magnetic moments [9]. Currently, industrially available calibration standards are rather dependent on materials that could be influenced by stress and temperature. When detection coils are specifically designed with significant nonlinear sensitivity, based on the presupposition of an ideal fabrication process that exactly conforms to the design coil winding and configuration, a VSM can also in principle be calibrated without a standard reference [10]. Nevertheless, in addition to their untraceability and the fact that the fabrication and assembly process of coil systems may deviate from the ideal design, such nonlinear detection coils have much smaller uniform saddle regions than standard VSMs, causing larger uncertainty due to high sensitivity dependence on the sample position. As a result, reliability over a wide range and traceability remains a problem for the accurate calibration of magnetic moments in VSM metrology.

Current-carrying coils can be used to replace a nickel ball and generate an adjustable magnetic dipole moment without demagnetization problems in any applied field [11], [12], [13]. In the American testing standard, the standard nickel sphere for saturation magnetization may be replaced by a coil of known dimensions and number of turns carrying a known dc current, where a multiple-layer coil may be used with the moments of each layer computed separately and added together [14]. Zieba and Foner [12] used the coil moment to confirm the image effect in a superconducting magnet with a magnetic moment range of 1 memu–1 emu by applying a 0.01–50-mA current. In an alternating gradient magnetometer, a coil moment was applied to surround the magnetic sample under testing and produce precision compensation [13]. Guy and Howarth [11] demonstrated that magnetic quadrupoles could also be measured in a VSM with calibration from a coil pair connected with a reverse current.

From a metrological point of view, for a reliable calibration method, the traceability path should be clearly established to the quantum standard, which is closer to Planck's natural unit system [15]. The construction of connections between the magnetic moment and quantum current standard is fundamentally important and valuable for improving the metrology of VSMs. Therefore, its reliability needs further exploration on accuracy, precision, and stability.

Generally, coils can be used for a separate standard of magnetic moment [14], but to what extent and how are the procedures for traceable calibrations with low error? Moreover, Ni spheres can reach 0.5% uncertainty when properly applied [8], but how far can the uncertainty be exceeded using an independent method? These two main issues motivated the current work.

Here, we study the calibration of current-carrying coils for tunable magnetic moments over a wide range to improve the accuracy and range of calibration for VSMs. From the standard current and flux calibration method, a magnetic moment is designed to experimentally connect quantum standards of the natural emission frequency. Differential magnetic moments driven by differential currents are used to avoid hysteresis and additive effects due to nonideal materials in coils. Moreover, with comparison to the Ni standard and slope method, wide-range calibration of the magnetic moment is performed *in situ* for VSMs without dependence on the field and materials, where the optimized uncertainty does not exceed 0.3% in the range of 2.5–3.7 memu.

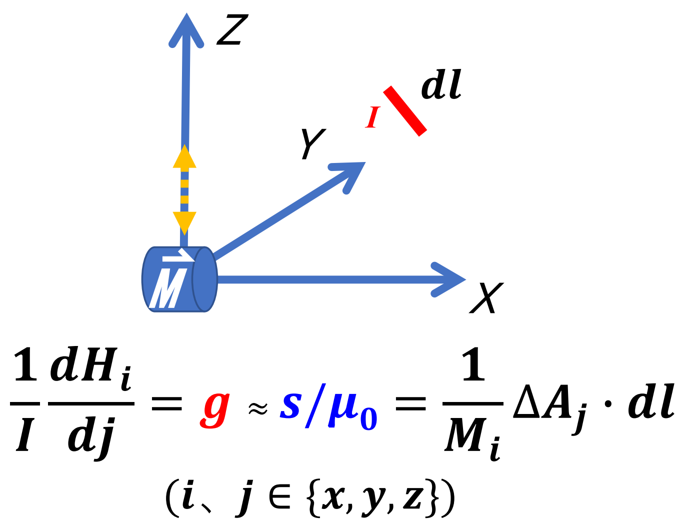

Fig. 1. Schematic of the reciprocal principle of VSM detection.

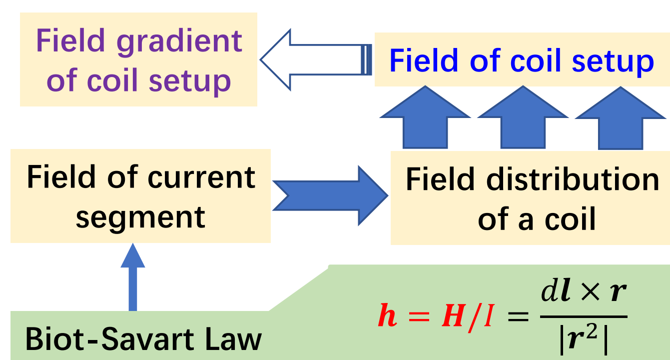

Fig. 2. Flowchart of the designing procedures for VSM detection.

II. Optimization of the Detection Coil Set

A. Designing Tool Based on the Reciprocal Principle

It is a substantial challenge to establish an absolute standard of magnetic moment connected to the quantum bench and simultaneously pursue low uncertainty. The detection coil set becomes the most important prerequisite for VSM calibration, so a designing tool is necessary to optimize the detection apparatus. Optimization of detection coils for VSM requires high sensitivity and a large saddle range. To obtain 0.5% error compared to the standards of Ni spheres and other fundamental quantities in the quantum benchmark, a large saddle range is critical. To make the magnetic moment comparable with standard Ni spheres, the coils for calibration are wound to be 2.5 mm in diameter and height. Considering the vibration amplitude of 1–4 mm, the designed saddle range along the Z-direction is set as 8 mm within 0.5% uniformity.

As studied by Mallinson, the reciprocal principle is effective for constructing the designing software [16]. The induction in a coil segment by the movement of the unit magnetic moment is related to the field gradient component in the corresponding directions of the unit current, as shown in Fig. 1, where g and s are the field gradient of the unit current and VSM sensitivity of the unit moment, respectively. After multiple integrations of field vectors produced by the unit current, the field distribution in the detection range and corresponding field gradient distribution of the unit current can be immediately obtained. Although both magnetic moment $\boldsymbol{M}$ and magnetic field $\boldsymbol{H}$ are the vectors with three components, M and H indicate M_x and H_x, respectively, with a simple way of symbolization, since VSMs usually apply x component of $\boldsymbol{H}$ and measure x component of $\boldsymbol{M}$. The calculation procedures are shown in Fig. 2, where Biot–Savart law is the starting point. Corresponding to the optimization requirement on high sensitivity and large saddle range, two key quantities for our VSM studies are calculated according to the following equations: total gradient of unit current g_{xz} and relative deviation of the gradient δg_{xz}

$$s/\mu_0 \approx g_{xz} = \sum_{\text{coil array}} \sum_{\text{each coil}} \frac{dH_x}{Id_z} \tag{1}$$

$$\delta g_{xz} = \frac{\max\{g_{xz}(R)\} - \min\{g_{xz}(R)\}}{\overline{g_{xz}(R)}} \times 100\%. \tag{2}$$

The default range [R in (2)] to calculate δg_{xz} is ± 2 mm along the Z-direction in the center of the standard four detection coils, as shown in Fig. 3(a).

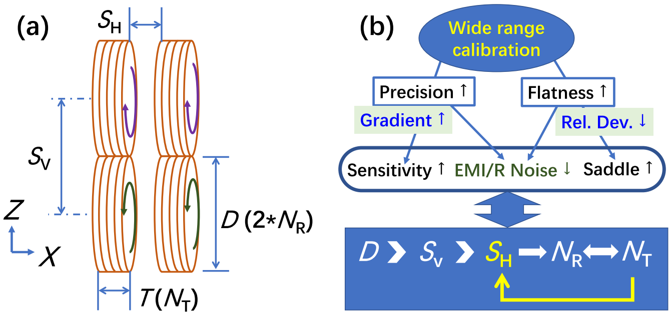

Fig. 3. (a) Structure and configuration of the VSM detection coils and (b) flowchart for the structure optimization plan.

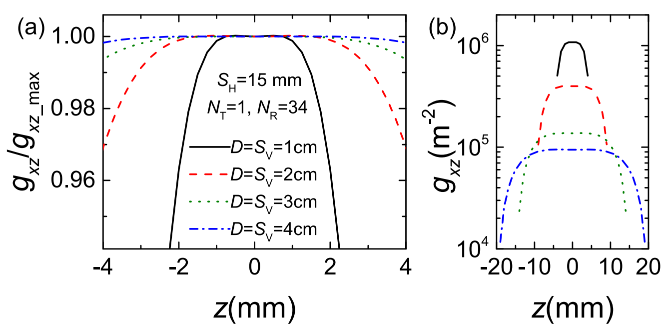

Fig. 4. Relative gradient dependence on positions along the Z center line for several main diameters and vertical spacing, while the horizontal spacing and winding parameters are identical. (a) Normalized gradient. (b) Absolute gradient.

B. Optimizing Plan Based on Structures

As shown in Fig. 3(a), conventional four coils are used in this study, where the rotation arrows show the relative direction of the coil array via orientation and electrical connection. There are five main parameters in the structure and configuration for VSM detection coils: main diameter D, vertical spacing S_V, horizontal spacing S_H, radial winding number N_R, and winding layers N_T. To realize high precision and high uniformity in the VSM saddle range in a convergent manner, these parameters are sequentially optimized, and S_H must be reoptimized when the winding parameters change, as indicated in Fig. 3(b). The optimizing procedures are further described in Sections II-C–II-G.

C. Main Diameter

The maximum saddle range is determined by the main diameter of all coils. As shown in Fig. 4, the coils with a diameter of 3 cm are suitable for <0.5% uncertainty in the 8-mm range along the Z-direction, where the sensitivity is approximately 13% of that from 1-cm coils. For a coil set with the main diameter of 4 cm, although the saddle range is more sufficient, its sensitivity decreases to <9% of that from 1-cm coils.

D. Vertical Spacing

Vertical spacing S_V is obviously no less than the main diameter, and Fig. 5 shows that both gradient coefficient and uniformity decrease when S_V increases. Therefore, S_V should be directly following the main diameter.

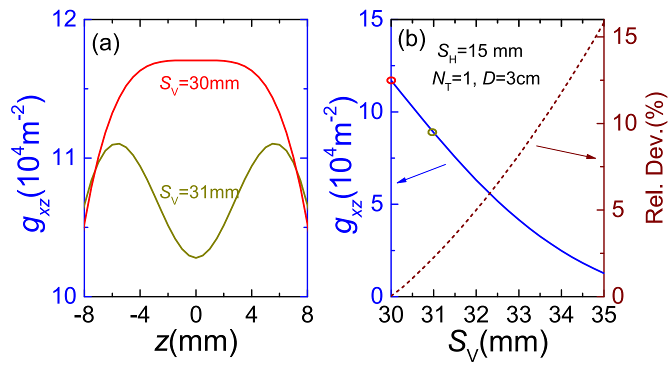

Fig. 5. Gradient coefficient and its deviation dependence on positions along the (a) Z center and (b) vertical spacing.

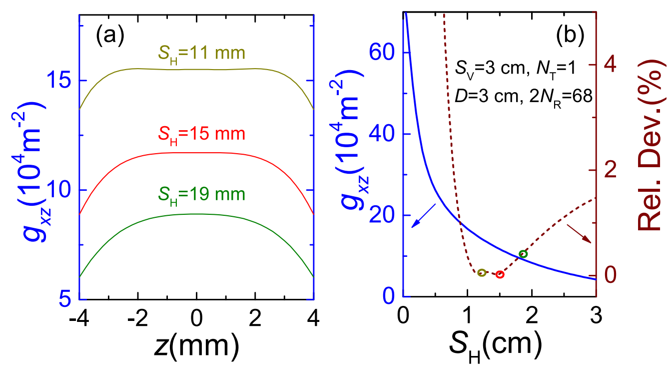

Fig. 6. Gradient coefficient and its deviation dependence on positions along the (a) Z center and (b) horizontal spacing.

E. Horizontal Spacing

Compared to S_V, the horizontal spacing S_H requires optimization. As shown in Fig. 6, the gradient coefficient decreases when S_H increases, but its deviation is minimal at maximal uniformity. Therefore, S_H should be reoptimized whenever the winding parameters change.

F. Radial Winding Number

Radial winding number N_R depends on the main diameter of the coils and wire diameter. A larger radial winding number can produce a higher gradient coefficient, but the electrical resistance will increase and introduce thermal noise. Therefore, the best N_R should be optimized by the total resistance of the winding coil (<500 Ω), which is calculated from the integrated length and diameter. Since N_R can jointly influence the uniformity, as shown in Fig. 7, the best S_H should refresh upward after N_R increases.

G. Winding Layers

Proper winding layers N_T and the corresponding thickness of coils must be found for mechanical reason and better uniformity. As shown in Fig. 8, S_H refreshes downward after N_T increases, which is opposite to N_T, as discussed in the previous section. Moreover, N_T is also a parameter for calculating the resistance of the coils. As a result, N_T and N_R

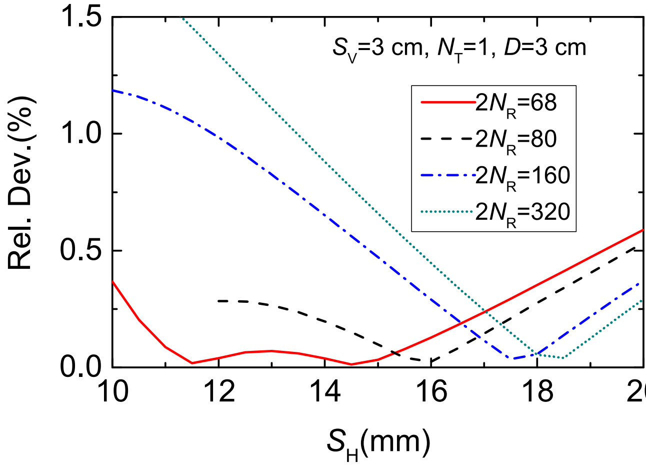

Fig. 7. Gradient deviation dependence on the horizontal spacing with several radial winding numbers.

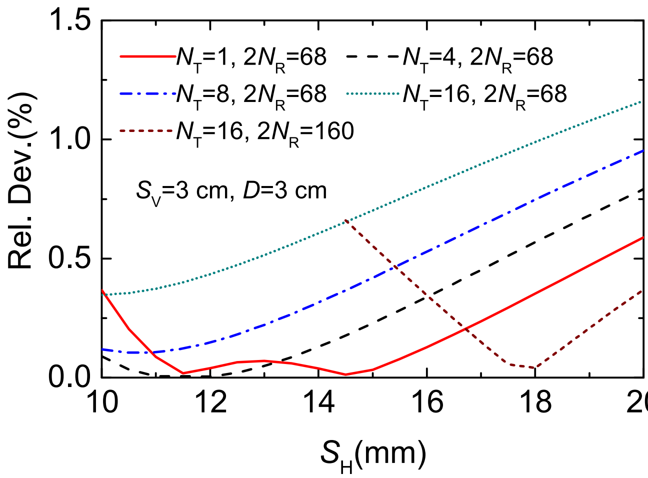

Fig. 8. Gradient deviation dependence on the horizontal spacing with several combinations of the radial winding number and winding layers.

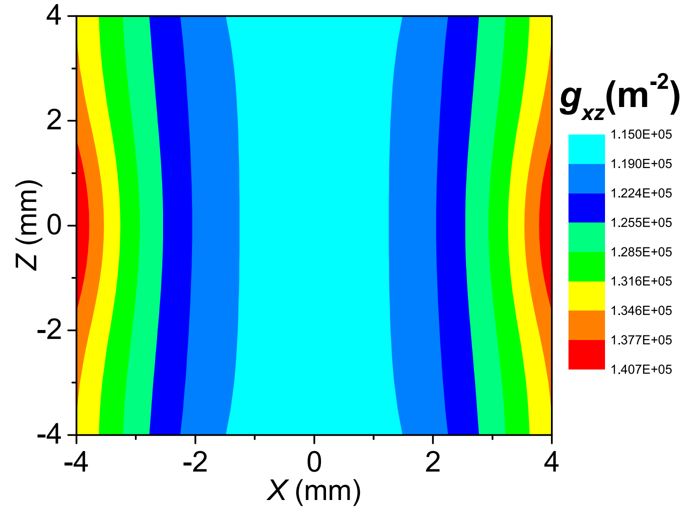

Fig. 9. Distribution of the gradient coefficient in the center XZ plane for the VSM coil set with $D = S_V = 3$ cm, $S_H = 15$ mm, $N_R = 34$, and $N_T = 1$.

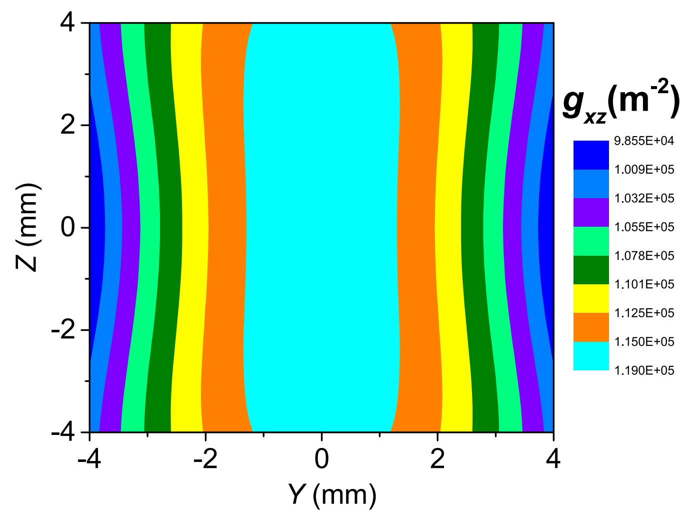

Fig. 10. Distribution of the gradient coefficient in the center YZ plane for the VSM coil set with $D = S_V = 3$ cm, $S_H = 15$ mm, $N_R = 34$, and $N_T = 1$.

are simultaneously optimized to refresh the best S_H in this work.

H. Three-Dimensional Saddle Range

Since moment coils always have three dimensions, it is interesting to show the saddle range in 3-D for availability checking. Figs. 9–11 have depicted the uniformity of gradient coefficient g_{xz} in three main center planes. The saddle range has the largest size along the Z-direction, while the uniform range along the X- and Y-directions is approximately 3 mm, which is sufficient for the standard Ni spheres and moment coils studied in this work.

I. Summary of VSM Coil Designing

The VSM saddle range can be realized by designing D, S_V, S_H, N_R, and N_T sequentially, as indicated in Fig. 3, with respect to the gradient coefficient, uniformity, and coil resistance. The most important parameter should be horizontal spacing S_H, which is the only parameter that can be optimized after the coils have been made. Fortunately, as discussed previously, for interchangeable coils, even D, S_V, N_R, and N_T have been fixed in a suitable range; thus, one may obtain suitable uniformity and sensitivity by finely adjusting the horizontal spacing S_H.

The inner diameter D_I of the coils has not been discussed. In fact, a smaller inner diameter corresponds to greater effective space utilization of the coil, which helps improve the sensitivity and uniformity, as shown in Fig. 12. During the fabrication of coils, the actual D_I inevitably has a certain size. However, Fig. 12 shows that the gradient deviation is insensitive to the inner diameter within 4 mm for coils with a main diameter of 3 cm. Therefore, D_I is not considered as one of the optimization parameters in this work.

III. Calibration Principle

To improve the reliability and traceability of magnetic moments over a wide range, current-driven coils are in

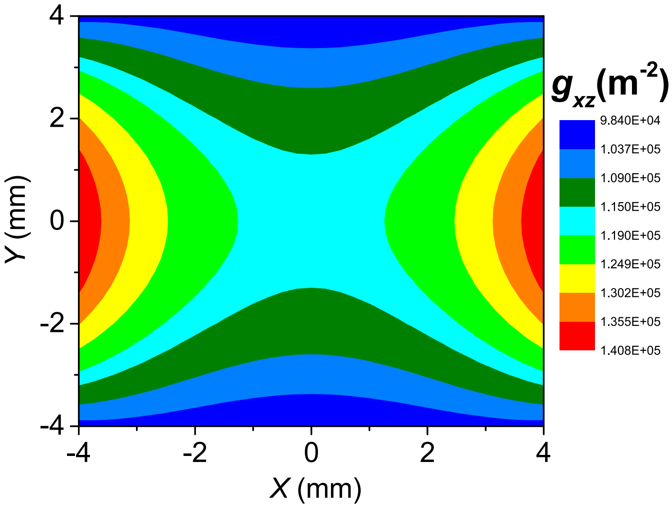

Fig. 11. Distribution of the gradient coefficient in the center *XY* plane for the VSM coil set with $D = S_V = 3$ cm, $S_H = 15$ mm, $N_R = 34$, and $N_T = 1$.

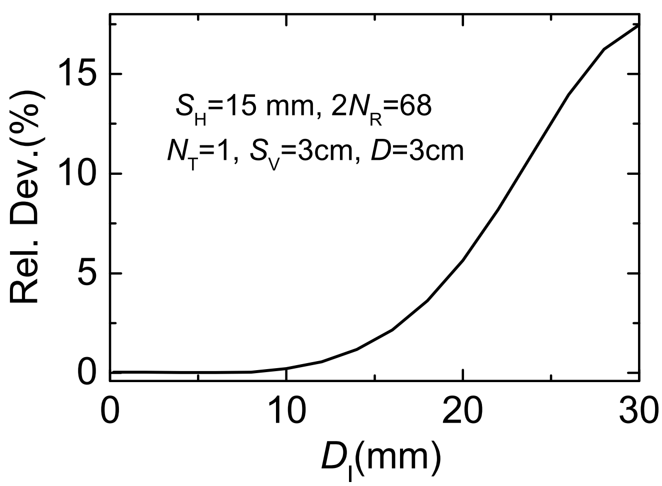

Fig. 12. Gradient deviation dependence on the inner hole diameter of the VSM coil set with $D = S_V = 3$ cm, $S_H = 15$ mm, $N_R = 34$, and $N_T = 1$.

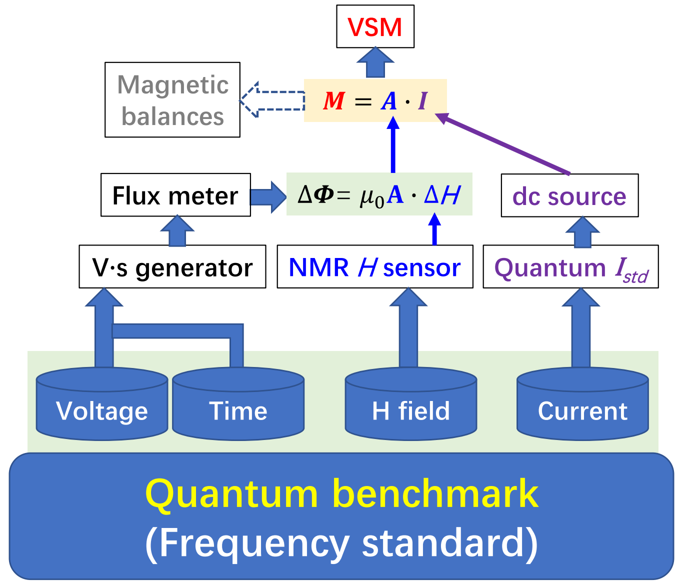

Fig. 13. Principle diagram for the traceable calibration of the magnetic moment.

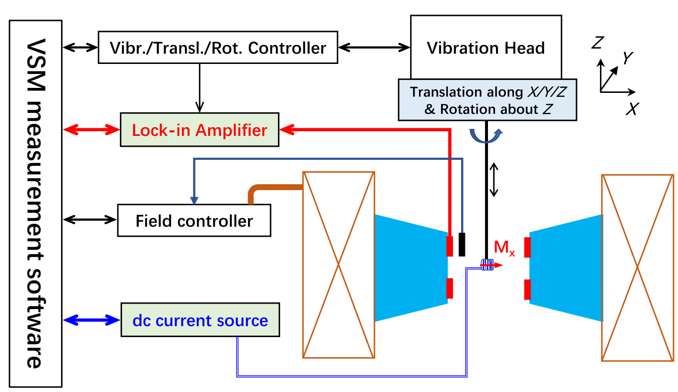

Fig. 14. Block diagram of the measuring electronics and controlling units for a VSM with a current-driven coil as the magnetic moment standard; the positional relationship is only for illustration, and the size is not proportional to that of the actual system.

principle more suitable than magnetic materials, as they have the significant advantage of environmental insensitivity when properly applied. Coils have been used as a magnetic moment standard for decades [11], [12], [13], [14]; unfortunately, clear data are lacking, so it is worthwhile to clarify the principle and application range of this standard. As shown in Fig. 13, the magnetic moment is composed of an electrical current and its winding area when a coil is used. To establish a path to the quantum benchmark, the winding area and dc current are calibrated *in situ* using a fluxmeter and quantum current standard, respectively. The fluxmeter is easily traceable to the quantum standard via a voltage-second generator and nuclear magnetic resonance (NMR) for the magnetic flux and magnetic field, respectively. In addition, the magnetic moment can be transmitted *ex situ* to the quantum standard using another possible method of a magnetic balance, which is suitable for auxiliary checking, but a strict proof of the moment-force path implies difficulty in simultaneously tracing the magnetic gradient and force to the quantum platform. Therefore, to show the reliability and traceability of the magnetic moment standard based on current-driven coils, this work investigates its calibration process, evaluates its uncertainty, and compares its usability with that of well-known standards of Ni spheres.

IV. Implementation of the Calibration Setup

The calibration setup is modified from that of a conventional VSM, as shown in Fig. 14, where the main measurement part includes a displacement module to control vibration and translation of the sample (Keyence IL-030 as a displacement monitor), a field controller with a combined temperature and magnetic field sensor (EastChanging P9060), and a moment recording unit composed of a four-coil detection set (5-mm saddle range of better than 0.1% uniformity) and a lock-in amplifier (SSI OE1022). To generate a current-driven magnetic moment standard, the Yokogawa 2553A is used to set a current of 10 nA–100 mA with an accuracy better than 100 ppm. To trace the winding area and external field of the coil sample

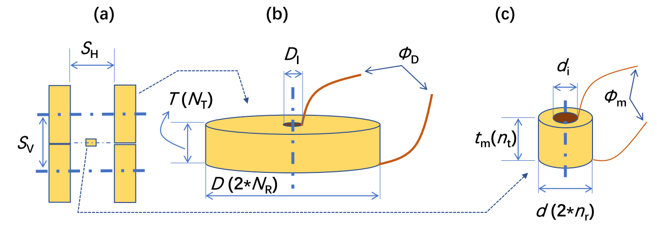

Coil Frame		Detection coil unit						Magnetic moment coil					
S_V	S_H	D	D_I	T	Φ_D	N_R	N_T	d	d_i	t_m	Φ_m	n_r	n_t
3.2 cm	1.47 cm	3.2 cm	4 mm	2.5 mm	120 μm	126	21	2.5 mm	1 mm	2.5 mm	50 μm	12	40

Fig. 15. Schematic configuration of (a) coil frame, (b) detection coil unit, and (c) magnetic moment coil, with dimensions listed in the table below the drawings, with respect to each label.

under meterage, the NIM TA102E and MetroLab PT2025 are applied to calibrate the magnetic flux and magnetic field, respectively. In addition to the centering operation for a conventional VSM, to ensure that the measured winding area is consistent with the design, the axis of the coil sample is aligned with the set field or X-direction by a sample holder with a transverse cylinder bore to tightly insert the coil and adjust the rotation angle about the Z-axis to maximize the magnetic flux.

To ensure a uniform range for moment calibration, magnetic moment coils should be designed to be sufficiently small, and the detection coil set has a correspondingly wide saddle range. The outer diameter and height were designed to be 2.5 mm for the moment coils to produce a wide range of moments. The corresponding detection coil set with a wide uniform range was then designed according to the reciprocal principle [16]. After the fabrication of 40 detection coils, four coils with close inductance were selected and embedded into a 3-D printed framework to mechanically fit taped electromagnet poles with 10 cm diameter and 35 mm spacing. The detailed designed parameters of the detection coil set and the moment coil are shown in Fig. 15 along with a schematic demonstration of their configuration.

V. Evaluation and Discussion

A. Intrinsic Uncertainty

Based on the ratio of flux change to flux density, the winding area can be experimentally determined *in situ* and used to set the magnetic moment. A coil with a measured winding area of 0.001240 m^2 was used to evaluate the precision and accuracy under various applied set currents. After the conventional VSM calibration process using the NIST saturation moment of an SRM 772a nickel sphere, the moment of the coil under an applied current was measured by subtracting the moment of the applied current from that of zero current. The relationship between the set moment and measured moment is shown in Fig. 16; it remains equal in the range of 1e-5–1e-1 emu across four orders of magnitude.

The original data of Fig. 16 are listed in Table I, which are statistically analyzed from raw measurements with the assumption of normal distribution. Raw data for all set moments are based on 30 independent measurements

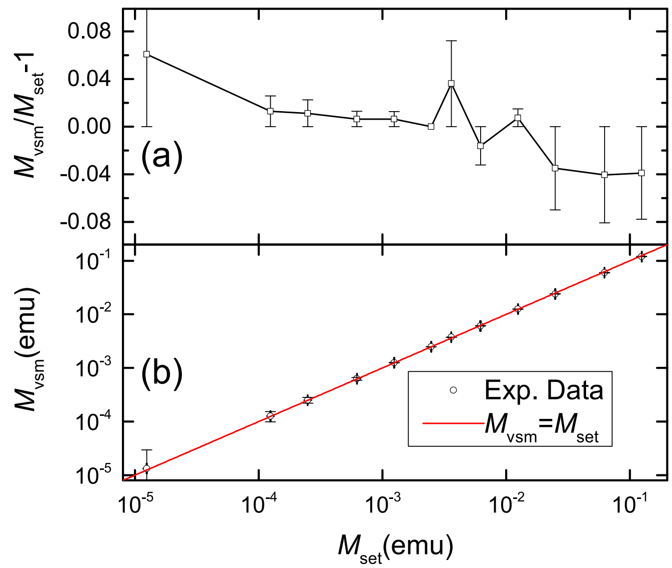

Fig. 16. Precision and accuracy of the measured moment difference in comparison with the set moment difference for a moment coil under various sets of currents, where (a) and (b) show relative and absolute precision, respectively. The magnetic field was not applied during the measurement process.

TABLE I

Precision and Accuracy of the Measured Moment Difference in Comparison With the Set Moment Difference for a Moment Coil Under Various Sets of Currents Without an Applied Magnetic Field

I (mA)	M_{set} (memu)	M_{meas} (memu)	δM_{meas} (memu)	Rel_Dev. (%)	Rel_Err. (%)
100	124	119.61	9.3E-01	0.78	-3.5
50	62	59.71	3.7E-01	0.62	-3.7
20	24.8	24.02	2.2E-01	0.93	-3.2
10	12.4	12.54	2.2E-02	0.18	1.1
5	6.2	6.1	9.6E-03	0.16	-1.6
3	3.72	3.73	8.8E-03	0.24	0.27
2	2.48	2.48	6.3E-03	0.25	0
1	1.24	1.25	4.7E-03	0.38	0.99
0.5	0.62	0.626	3.4E-02	5.4	1.0
0.2	0.248	0.252	3.0E-02	11.9	1.5
0.1	0.124	0.126	2.7E-02	21.6	1.7
0.01	0.0124	0.0132	1.6E-02	122.9	6.5

in 30 s for all set moments, except the moment range of 1.24–12.4 memu, where 3600 independent measurements were taken as raw data in 1 h. The precision (indexed by relative deviations) is below 0.5% in the range of 1.24–12.4 memu, and the accuracy is below 0.3% in the range of 2.5–3.7 memu.

The accuracy dependence on the set moment in Table I is plotted in Fig. 17, where low moments and high moments show positive and negative errors, respectively. The positive error in the small magnetic moment range is attributed to finite detection noise, such as thermal and electromagnetic interference. The negative error in the large magnetic moment range can be associated with the complex image effect, which is well known in VSM due to the high permeability of

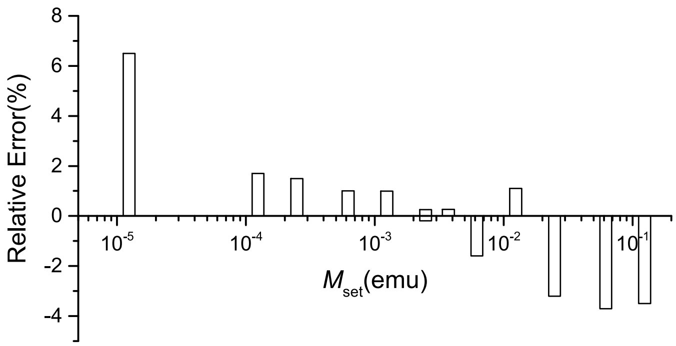

Fig. 17. Relative error dependence on the set magnetic moment, plotting from the last column of Table I. The error data of 2.48 memu were taken from the relative deviation because the measured error was zero.

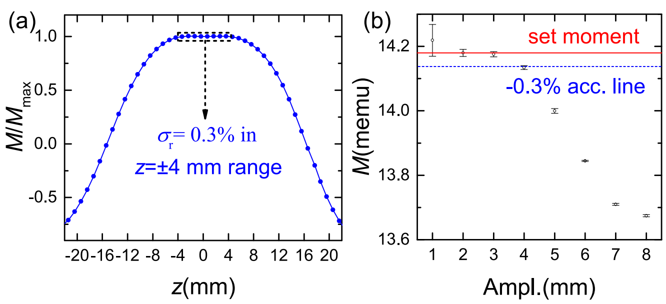

Fig. 18. Dependence of the magnetic moment on positions along the (a) Z center and (b) amplitudes.

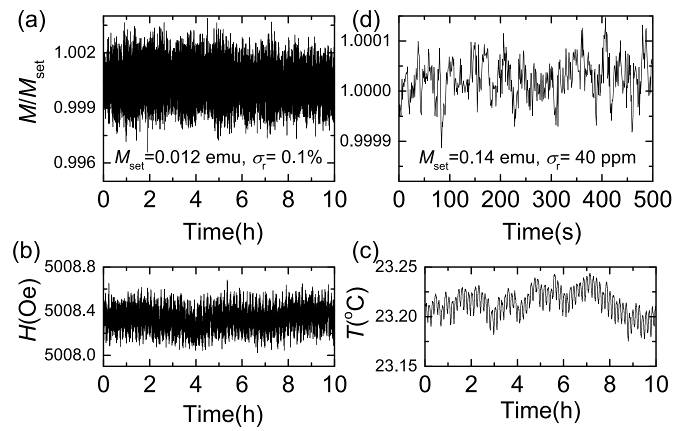

Fig. 19. Stability of the measured magnetic moment during the testing time, (a) and (b) in different time windows, where environmental conditions such as (c) field and (d) temperature vary with the same time period as that of (a).

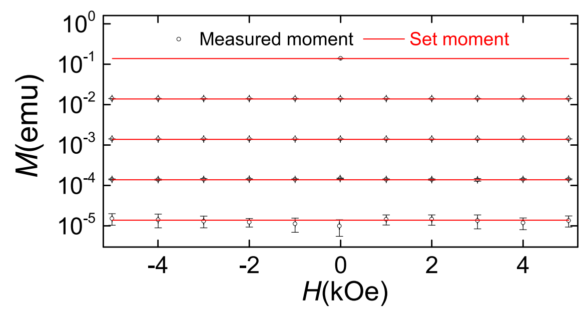

Fig. 20. Field dependence of the magnetic moment under various set currents.

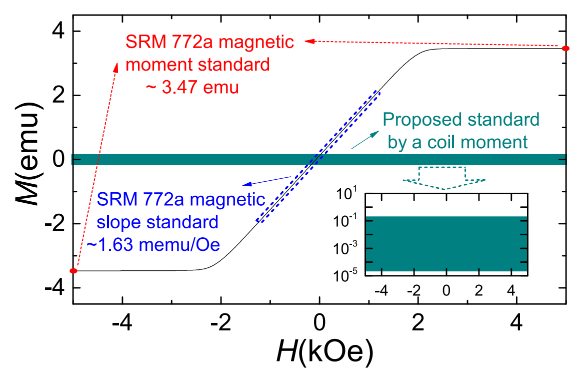

Fig. 21. Comparison of the current coil method with the saturated moment and slope method using standard nickel spheres in a wide range of magnetic fields and moments.

electromagnetic poles under a lower magnetic field, including the standard calibration field of the Ni sphere at approximately 5 kOe. Totally consistent calibration would be possible when replacing samples with a standard of the same shape/size, magnetic moment and external magnetic field. To push the accuracy and precision further, comprehensive exploration of the image effect is ongoing for moment calibration based on different coil shapes.

B. Environmental Compatibility

Position dependence is a well-known problem in VSM calibration. To solve this problem and make *in situ* calibration available, except for entering, the saddle range was designed to be approximately 8 mm in the Z-direction with a 0.3% relative standard error. The measured saddle curve is shown in Fig. 18(a), and it is largely consistent with the vibration–amplitude dependence curve in Fig. 18(b). The accuracy decreases sharply when the amplitude is greater than 5 mm, but the precision becomes worse when the amplitude is lower than 1 mm. Therefore, the reliable amplitude for calibration and measurement is between 2 and 4 mm to ensure a relative moment error below 0.3%.

The stability was also evaluated for typical applied moments. As shown in Fig. 19(a)–(c), in a period of 10 h, the relative standard error was approximately 0.3% for a set moment of 0.012 emu, where the deviation of the field and temperature was 0.4 Oe and 0.1°, respectively. When the applied current was increased, the relative standard error decreased, as shown in Fig. 19(d). In a period of 500 s, the relative standard error was approximately 40 ppm for a set moment of 0.14 emu.

C. Comparison With Standards

The wide field and moment range are the most interesting advantages of the proposed standard of the magnetic moment of a current coil. As shown in Fig. 20, the measured moments agree quite well in a field range of ±5 kOe and moment range of four orders of magnitude.

Compared to the conventional VSM standard using nickel spheres, as shown in Fig. 21, the saturated moment and slope methods are available at approximately 5 kOe and within a range of ±1 kOe, respectively, while the proposed standard is independent of the magnetic field in the moment range of ±0.14 emu. The moment range could be increased further if heat exchange conditions were applied to prevent coil damage under a large applied current.

In principle, the moment range of nickel spheres could be adjusted by changing the diameter. Nevertheless, in the range of 1e-5–1e-1 emu, microspheres are difficult to fabricate for standard usage. The field-dependent behavior of nickel spheres makes *in situ* calibration impractical. Moreover, fundamentally, magnetic property-based standards have no path to recognize quantum benchmarks, which is a benefit of the proposed coil-based magnetic standard. High uncertainty and fusing may become possible due to electromagnetic noise in a moment range below 1e-5 emu and irreversible heating damage in a moment range above 1e-1 emu, respectively. However, magnetic moments below 1e-5 emu and above 1e-1 emu are expected, when measures of noise inhibition and active cooling are applied, respectively.

In order to further improve the calibration accuracy and precision, it is worth mentioning NIM-2 joule balance with 240-ppb uncertainty [17] and NIST-3 watt balance within 77 ppb for ten years [18], where the control of magnetic moment and magnetic field is remarkable to follow. With the integrated use of precise electromagnetic gradient design, superconducting current, and interference suppression technology, the ultimate calibration uncertainty is expected to reach 20 ppb [17], [18].

As mentioned in the previous sections, a special detection coil set with a wide saddle range is needed, while the reliability is not guaranteed by conventional VSM detection coils of a narrower saddle range. Moreover, the best uncertainty range may change when the environment and VSM detection configuration vary, so the traceability process is difficult outside of metrology organization. Therefore, this method is unfortunately not directly used for mass diffusion for industrial sites. Nevertheless, for industrial usage of this method, transmission and recalibration of Ni spheres are more convenient from metrology organizations to end manufactory users.

The proposed moment coil method is complementary for the metrology system of magnetic moment with respect to Ni spheres, which are not replaceable at the moment because of convenience and simplicity. The main motivation and contribution of the current work is establishing a bridge between Ni spheres and the quantum benchmark and extending the calibration range in a continually tunable manner with an independent configuration.

VI. Conclusion

In situ calibration of a wide-range magnetic moment for VSMs is established without dependence on the field and materials, where the relative uncertainty does not exceed 0.3% within the range of 2.5–3.7 memu. Because this method can trace back to a recognized quantum benchmark, it is expected to be applicable in the standard metrology of magnetic moments. For industrial usage, standard transmission and recalibration of Ni spheres are more convenient from metrology organization to end manufactory users; in fundamental science studies, the precision and accuracy can be improved as soon as there is improvement in noise inhibition and shape optimization.

References

[1] G. W. Van Oosterhout, "A rapid method for measuring coercive force and other ferromagnetic properties of very small samples," *Appl. Sci. Res., B*, vol. 6, no. 1, pp. 101–104, Dec. 1957, doi: 10.1007/BF02920365.

[2] S. Foner, "Versatile and sensitive vibrating-sample magnetometer," *Rev. Sci. Instrum.*, vol. 30, no. 7, pp. 548–557, Jul. 1959, doi: 10.1063/1.1716679.

[3] P. J. Flanders and C. D. Graham, "DC and low-frequency magnetic measuring techniques," *Rep. Prog. Phys.*, vol. 56, no. 3, pp. 431–492, Mar. 1993, doi: 10.1088/0034-4885/56/3/002.

[4] C. D. Graham, "High-sensitivity magnetization measurements," *J. Mater. Sci. Technol.*, vol. 16, no. 2, pp. 97–101, Jan. 2000.

[5] F. Fausto, *Measurement and Characterization of Magnetic Materials*. Amsterdam, The Netherlands: Elsevier, 2004.

[6] F. Fiorillo, "Measurements of magnetic materials," *Metrologia*, vol. 47, no. 2, pp. S114–S142, Apr. 2010, doi: 10.1088/0026-1394/47/2/S11.

[7] *International Compar–Ison of Measurements of the Magnetic Moment*, Geneva, Switzerland, IEC Standard 62797, 2013.

[8] W. E. Case and R. D. Harrington, "Calibration of vibrating-sample magnetometers," *J. Res. Nat. Bureau Standards-C Eng. Instrum.*, vol. 70, no. 4, pp. 255–262, Oct./Dec. 1966, doi: 10.6028/jres.070C.024.

[9] A. Riminucci, M. Uhlarz, R. De Santis, and T. Herrmannsdörfer, "Analytical balance-based Faraday magnetometer," *J. Appl. Phys.*, vol. 121, no. 9, Mar. 2017, Art. no. 094701, doi: 10.1063/1.4977719.

[10] U. Außerlechner, W. Steiner, and P. Kasperkovitz, "Calibration of vibrating sample magnetometers independent of reference samples," *Meas. Sci. Technol.*, vol. 7, no. 11, pp. 1574–1578, Nov. 1996, doi: 10.1088/0957-0233/7/11/005.

[11] C. N. Guy and W. Howarth, "Non-uniform magnetisation and the vibrating-sample magnetometer," *J. Phys. C, Solid State Phys.*, vol. 11, no. 8, pp. 1635–1650, Feb. 2001, doi: 10.1088/0022-3719/11/8/023.

[12] A. Zieba and S. Foner, "Superconducting magnet image effects observed with a vibrating sample magnetometer," *Rev. Sci. Instrum.*, vol. 54, no. 2, pp. 137–145, Feb. 1983, doi: 10.1063/1.1137359.

[13] T. Frey, W. Jantz, and R. Stibal, "Compensating vibrating Reed magnetometer (invited)," *J. Appl. Phys.*, vol. 64, no. 10, pp. 6002–6007, Nov. 1988, doi: 10.1063/1.342132.

[14] *Standard Test Method for Saturation Magnetization or Induction of Non Metallic Magnetic Materials*, ASTM, Pennsylvania, PA, USA, Standard A894, 2011.

[15] CEC General Conference on Weights and Measures. *On the Revision of the International System of Units (SI)*. Accessed: Jul. 2022. [Online]. Available: https://www.bipm.org/en/committees/cg/cgpm/26-2018

[16] J. Mallinson, "Magnetometer coils and reciprocity," *J. Appl. Phys.*, vol. 37, no. 6, pp. 2514–2515, May 1966, doi: 10.1063/1.1708848.

[17] J. Xu *et al.*, "Research on the effect of the external magnetic field in the Joule balance at NIM," *Metrologia*, vol. 55, pp. 392–403, May 2018, doi: 10.10.1088/1088/1681681-7575/aabec2-7575/aabec2.

[18] S. Schlamminger, R.L. Steiner, and D. Haddad, "A summary of the Planck constant measurements using a Watt balance with a superconducting solenoid at NIST," *Metrologia*, vol. 52, pp. L5–L8, Feb. 2015, doi: 10.1088/0026-1394/52/2/L5.

Zhigao Zhang received the bachelor's and master's degrees from Tianjin University, Tianjin, China, in 1992 and 1995, respectively.

He joined the National Institute of Metrology, Beijing, China. His current research interests include magnetic material hysteresis loop measurement, permanent-magnet magnetic moment measurement, and weak magnetic permeability measurement.

Zhiyi Xu received the M.S. degree from the University of Science and Technology Beijing (USTB), Beijing, China, in 2009, and the Ph.D. degree from the Institute of Physics (IOP), Chinese Academy of Sciences, Beijing, in 2013.

From 2013 to 2020, he worked as an Electromagnetic Metrologist with the National Institute of Metrology (NIM), Beijing. After 2020, he joined the Institute of Physics and Ganjiang Innovation Academy (GIA), Chinese Academy of Sciences. His research interests include magnetic materials and applications, magnetic measuring technology and standardization.

Jian He received the bachelor's degree from the Northeastern University, Shenyang, China, in 2002, and the master's degree from the University of Science and Technology Beijing (USTB), Beijing, China, in 2005.

Then he joined the National Institute of Metrology, Beijing. His current research interests include magnetic material measurement and standardization technology.

Mr. He is a member of International Electrotechnical Commission (IEC) TC68 working group 5.

Jun Lu received the B.S.M.S.E degree from the Huazhong University of Science and Technology, Wuhan, China, in 2003, and the Ph.D. degree from the University of Science and Technology Beijing, Beijing, China, in 2010.

From 2007 to 2009, under funding support from the China Scholarship Council, he presented his Ph.D. thesis with the University of Augsburg, Augsburg, Germany, on broadband electrodynamic measurement techniques for multiferroics with applications to bismuth ferrite crystals. After Post-Doctoral Researcher with the Technical Institute of Physics and Chemistry, he joined the State Key Laboratory on Magnetism, Institute of Physics, Chinese Academy of Sciences, Beijing. His current research interests include lock-in frequency meters, electromagnetic property inversion, and measurement devices for magnetic phenomena.